

A statistical study of the spectra of very luminous IRAS galaxies

I. Data

H. Wu¹, Z.L. Zou¹, X.Y. Xia² and Z.G. Deng³

¹ Beijing Astronomical Observatory, Chinese Academy of Sciences, Beijing 100080, China

² Department of Physics, Tianjin Normal University, Tianjin 300074, China

³ Department of Physics, Chinese Academy of Sciences Graduate School, Beijing 100039, China

Received ; accepted

Abstract. ¹

This paper presents the results of spectral observations for the largest complete sample of very luminous IRAS galaxies obtained to date. The sample consists of those 73 objects for which $\log(L_{\text{IR}}/L_{\odot}) \geq 11.5$ ($H_0 = 50 \text{ km s}^{-1} \text{ Mpc}^{-1}$, $q_0 = 0.5$) and $\text{mag} \leq 15.5$, and was extracted from the 2 Jy IRAS redshift catalog. All the spectra were obtained using 2.16m telescope of Beijing Astronomical Observatory during the years 1994-1996. A total of 123 galaxy spectra were obtained with spectral ranges of 4400Å to 7100Å and 3500Å to 8100Å at resolutions of 11.2Å and 9.3Å respectively. In addition to the 73 spectra for sample galaxies, we also present spectra for ten non-sample galaxies and a further 40 for the companions of sample galaxies. The data presented include nuclear spectrum and the parameters describing the emission lines, absorption lines and continua as well as DSS images and environmental parameters.

Key words: luminous infrared galaxies – spectra – environment

1. Introduction

The Infrared Astronomical Satellite (IRAS) all-sky survey provided a large database (IRAS Point Source Catalog, Version 2, 1988) of infrared galaxies. Based on recently completed redshift surveys of IRAS galaxies, statistical

spectroscopic analysis of very luminous IRAS galaxy samples can now be performed. Sanders et al. (1988) have already studied the spectra of a small sample of ten ultraluminous IRAS galaxies selected from IRAS Bright Galaxy Survey (BGS) of Soifer et al. (1986). Recently Kim et al. (1995) completed a spectroscopic survey based on a large sample of luminous IRAS galaxies that was extracted from both the BGS and infrared warmed catalogs. However, the infrared luminosity range of Kim et al.'s sample is from $10^{10.5} L_{\odot}$ to $10^{12.5} L_{\odot}$ and it therefore can not represent very luminous IRAS galaxies.

This paper presents the spectroscopic data for a large complete sample of very luminous IRAS galaxies (VLIRGs), extracted from 1.936 Jy Redshift Survey of Strauss et al. (1992). The DSS images are also presented, here. A detailed analysis of the spectra and environment will be presented in paper II (Wu et al. 1997).

2. Sample selection

Strauss et al. (1990) selected 5014 objects from the IRAS database (IRAS Point Source Catalog, Version 2, 1988) according to the criteria:

1. $f_{60} > 1.936 \text{ Jy}$
2. $f_{60}^2 > f_{12} f_{25}$
a color criterion distinguishing galaxies from objects in the Galaxy
3. Galactic latitude $|b| > 5^\circ$

Strauss et al. (1992) then went on to publish the redshifts of the 2658 objects which were galaxies (here after the 2Jy samples).

Our VLIRG sample is a subset of the 2Jy sample. Considering the observatory site, instruments and possible observation times, we selected galaxies according to the following criteria:

Send offprint requests to: H. Wu

¹ Table 2-4 and Figure 4,9 are only available in electronic form at the CDS via anonymous ftp to cdsarc.u-strasbg.fr (130.79.128.5) or via http://cdsweb.u-strasbg.fr/Abstract.html.

1. $\delta \geq 0^\circ$
2. $\log(L_{\text{IR}}/L_\odot) \geq 11.5$
($H_0 = 50\text{kms}^{-1}\text{Mpc}^{-1}, q_0 = 0.5$)
3. $\text{mag} \leq 15.5$

Here the magnitudes are from the 2Jy catalog. These criteria guarantee S/N ratios good enough for spectroscopic classification. 73 of 2Jy-catalogue VLIRGs met these criteria.

On account of the low S/N at $12\mu\text{m}$ and $25\mu\text{m}$ for some of sources in 2 Jy sample, we used Dennefeld et al.'s (1986) formula for calculating the infrared flux, between $42.5\mu\text{m}$ and $122.5\mu\text{m}$:

$$F_{\text{IR}} = 1.75[2.55S_{60} + 1.01S_{100}]10^{-14}\text{Wm}^{-2} \quad (1)$$

where, S_{60} and S_{100} are the fluxes at $60\mu\text{m}$ and $100\mu\text{m}$ respectively.

The infrared luminosity is therefore:

$$L_{\text{IR}} = 4\pi D^2 F_{\text{IR}} \quad (2)$$

for each object, where D is the distance from the Galactic center.

3. The sources lists and general properties

Table 1 lists the 83 target galaxies, of which 73 belong to the complete sample. Of the other ten objects in brackets, four of them have slightly lower infrared luminosities than $10^{11.5} L_\odot$ and six are fainter than our magnitude limit ($\text{mag} > 15.5$). This table presents the infrared luminosities in unit of L_\odot , magnitudes and redshifts. All of these data were derived from the 2Jy catalog, except that in the case of IR09517+6954 (M82). We can not use redshift as a distance indicator on account of the proximity. For this reason, we adopted the distance value given by Tully (1988). These objects flagged with asterisks in column 1 are the sources which are also included in the IRAS Bright Galaxy Sample ($S_{60} > 5.24\text{Jy}$) of Kim et al.(1995). A detailed comparison between these two samples will be made in paper II.

The spatial distribution of the 73 sample galaxies on the sky is shown in Fig.1. The dotted curve is the celestial equator. The scarcity of objects near galactic declination $b \sim 0^\circ$ is due to the matching Zwicky catalog (1961-1968) which misses galaxies at low latitude.

Fig.2 shows the sample distribution as a function of redshift. The solid boxes represent the complete sample, while the dotted boxes include the other ten sources. It is clear that the redshifts concentrate in the range 0.02 to 0.04. The median value is 0.0324 (corresponding to a recession velocity 9700kms^{-1}) which is larger than the value 5900kms^{-1} obtained by Kim et al.(1995) for their sample.

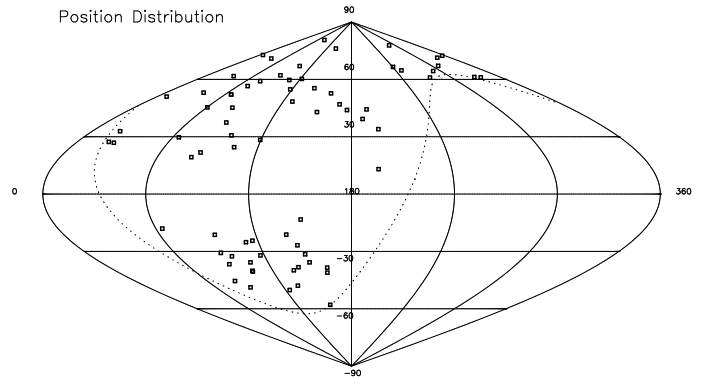


Fig. 1. The distribution of very luminous IRAS galaxies in the sky shown in equal area projection using Galactic coordinates.

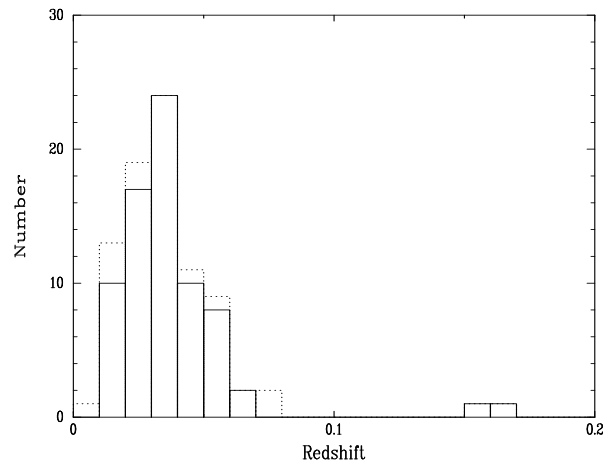


Fig. 2. Distribution of redshifts. The solid boxes represent our complete samples while the dotted boxes include the other ten galaxies.

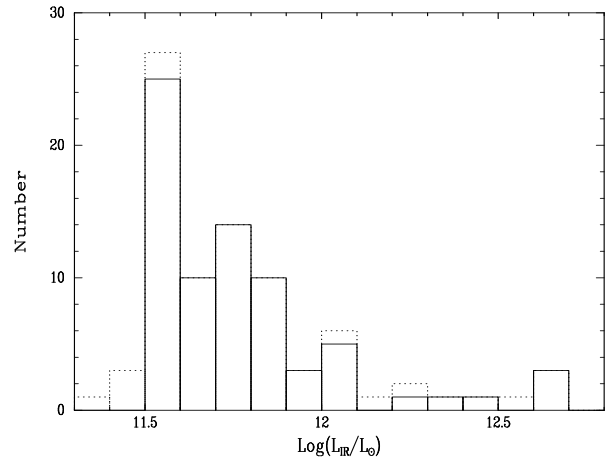


Fig. 3. Distribution of infrared luminosities. The solid and dotted boxes represent the same galaxies as they do in Fig.2.

The infrared luminosity distribution is shown in Fig.3. The solid and dotted boxes correspond to the same samples as in Fig.2. The counts decrease rapidly as the infrared luminosity increases. Most of the galaxies have infrared luminosities $\log(L_{\text{IR}}/L_{\odot})$ between 11.5 and 12.0.

4. Spectroscopic observations

The spectroscopic observations were made between Apr.15, 1994 and Feb.15, 1996. We obtained a total of 123 galaxy spectra. All of the observations were made with 2.16m telescope at the Xinglong Station of Beijing Astronomical Observatory using Zeiss universal spectrograph with a grating of $195\text{\AA}/\text{mm}$ dispersion.

Before Nov.5, 1994, a Tek 512x512 CCD which covered a 2700\AA range from 4400\AA to 7100\AA at a resolution of 11.2\AA (2 pixels) was used. After that, a Tek 1024x1024 CCD which covered a 4600\AA range from 3500\AA to 8100\AA at a resolution of 9.3\AA (2 pixels) was employed.

In most cases, slit width of about $3''$ was chosen to match the typical seeing disc at Xinglong Station, but occasionally, the seeing disc was smaller than $2''$ or larger than $5''$. Thus may affect the spectral classification. Slit position angles of 90° were generally used. For objects with two close nuclei (separation $\leq 2'$), the slit was rotated such that two spectra could be obtained simultaneously.

The seeing was about $3''$ to $4''$ on most of the observation nights. In order to perform a relative flux calibration, KPNO standard stars were also observed on each night.

Table 2 lists the observations by target objects. The standard IRAS name, together with one upper case letters representing the individual components(See Fig.9 for identifications) are listed in Column 1. Column 2 to Column 10 give for each source: coordinates, observation date (Beijing Time), exposure time, airmass, slit width and position angle respectively. The sources flagged with ticks in Column 11 were observed during good weather condition.

5. Data reduction

All of the data reductions were performed using IRAF². The IRAF packages CCDRED, TWODSPEC and ONEDSPEC were used to reduce the long-slit spectral data. The CCD reductions included bias subtraction, flat-field correction and cosmic-ray removal. The dark counts were so low that their subtraction was not performed. We adopted Horne's (1986) avariance weighed algorithm in order to extract the spectra. As for the aperture size, we adopted similar method to that of Kim et al.(1995) to minimize the aperture-related effects on the nuclear spectra. The apertures were varied according to the redshift of the objects so that they approached diameters of 2 kpc ($H_0 = 50\text{kms}^{-1}\text{Mpc}^{-1}$) for galaxies with $z < 0.034$, but were fixed at $4''$ for objects at larger redshifts as the seeing was typically $3''$ to $4''$ and the pixel sizes was $1.3''$.

² IRAF is provided by NOAO

The only two exceptions were for IR12323+1549A and IR09517+6954 (M82) which are quite nearby and a 2 kpc aperture was too large for them.

An Fe-He-Ar lamp was used for the wavelength calibrations. More than 20 lines were used to establish the wavelength scale by fitting a first-order spline3 function. The accuracy of the wavelength calibration was better than 1\AA .

On most nights, more than two KPNO standard stars were used to perform the relative flux calibration. Atmospheric extinction was corrected using the mean extinction coefficients for the Xinglong station, that were measured out by BATC multi-color survey (Yan, 1995).

The telluric O_2 absorption bands at 6870\AA and 7620\AA did heavier effect on those emission lines at the similar observed wavelength. We therefore constructed an artificial - the spectrum of standard stars setting every wavelength to unity except these wavelength corresponding to the O_2 bands. Division by the artificial spectrum could therefore removed telluric absorption bands. In most cases, this technique worked well, especially for the band near 6870\AA . However in some cases, this correction seems not to have been very satisfactory and affected the measurement of the emission lines at 7620\AA .

6. Spectra obtained

Optical spectra are presented for all program objects in Fig.4. They have all been corrected for telluric absorption, though some of corrections were not as good as we would have thought.

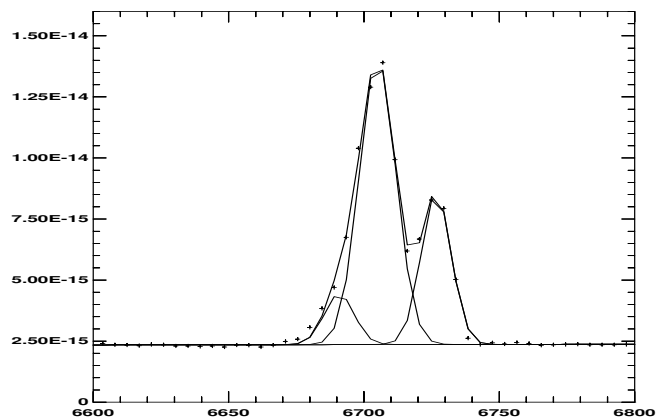


Fig. 5. Example of Gaussian fit for $\text{H}\alpha + [\text{NII}]\lambda 6584 + \lambda 6548$ emission. Three narrow Gaussian components are used. The pluses are observed data.

The measurements of emission line, absorption line and continuum strengths were performed within the IRAF environment using tasks (SPLOT and SPECFIT). For

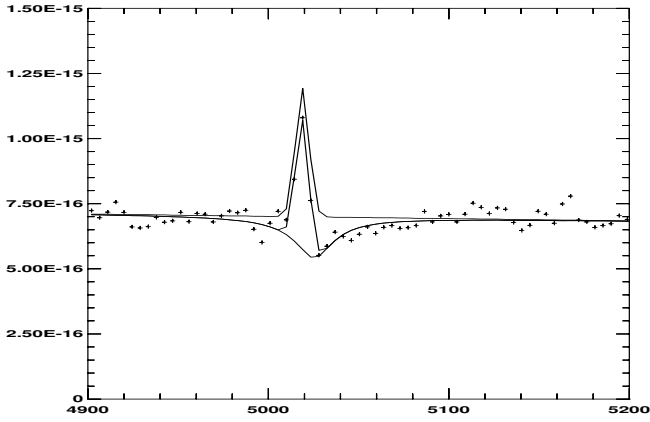


Fig. 6. Example of multi-component fit for the galaxies with strong Balmer absorption. One Lorentz absorption and one narrow Gaussian emission components are used.

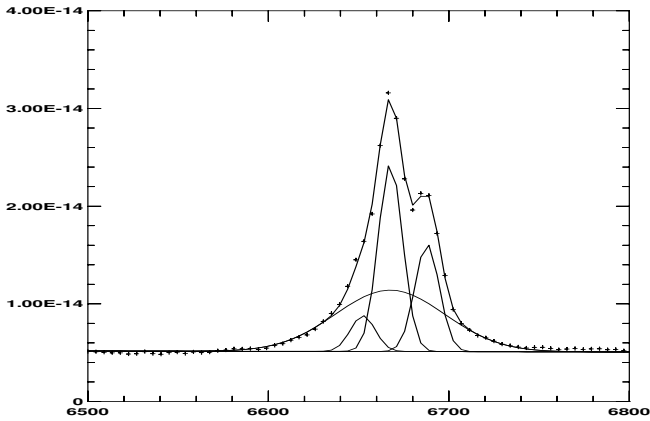


Fig. 7. Example of Gaussian fit for Seyfert 1s. One broad and three narrow Gaussian emission components are used.

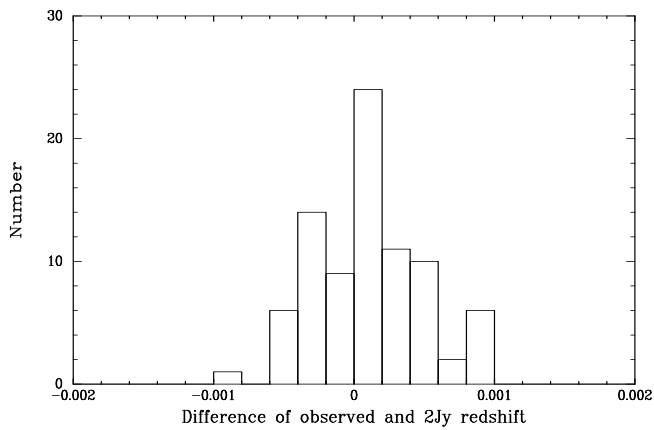


Fig. 8. Distribution of redshift differences between our data and the 2Jy redshift catalog.

isolated emission lines such as $[\text{OIII}]\lambda 5007$, $[\text{OII}]\lambda 3727$ and $[\text{OI}]\lambda 6300$, both Gaussian fitting and direct integral methods were used. For the blended lines such as $\text{H}\alpha$, $[\text{NII}]\lambda 6548, \lambda 6584$, and $[\text{SII}]\lambda 6716, \lambda 6731$ double lines, we employed a multi-Gaussian component method using task SPECFIT, to deblend them. There are three parameters for each Gaussian component: the central wavelength, the total flux and width of the emission line; and two parameters for each continuum component: the flux and the slope. In order to speed up the convergence, some limit conditions were adopted. For example, we fixed the center wavelengths of several components relate to one another. In Fig.5, for example, we used the simplex algorithm for the fitting and obtained the result via a chi-square minimization process. As for the spectra with obvious $\text{H}\beta$ absorption indicating an underlying stellar population, a similar method was used. Because of the coexistence of $\text{H}\beta$ emission and absorption, one emission and one absorption component were used for the $\text{H}\beta$ fitting. The wide absorption wings due to stellar populations often cause the absorption to be overestimated if Gaussian model is adopted. To solve this problem, we adopted the Lorentz model as shown in Fig.6, and the results seem better. Some of our sample galaxies are Seyfert-like, and their spectra could not fitted well with only single Gaussian component for each of $\text{H}\alpha$, $\text{H}\beta$. In those case, we combined one narrow ($< 1000\text{kms}^{-1}$) and one broad ($> 1000\text{kms}^{-1}$) Gaussian component as shown in Fig.7.

The relative emission-line fluxes are listed in Table 3 for all objects. The typical uncertainty in these measurement is about 10%. Colons (:) and semicolons (;) indicate values with relative uncertainties at about 30% and 50% respectively. For the line $[\text{OII}]\lambda 3727$, we could not obtain a value with an uncertainty of less than 20%, because it was at the blue end of the spectra, which can be affected by the low Q.E., lower S/N and poor flux calibration. In some cases, $[\text{OI}]\lambda 6300$ lines were heavily affected by the nearby emission lines $[\text{SIII}]\lambda 6312$ which could increase the uncertainty. The telluric absorption bands 6870\AA and 7620\AA was also enlarge the uncertainty in the measurement of lines near them, despite the corrections performed. The double lines $[\text{SII}]\lambda 6716, \lambda 6733$, could sometimes be separated, but when this was not possible, only the combined values are given.

The measured redshifts, observed $\text{H}\alpha$ fluxes, equivalence widths of $\text{H}\alpha$ emission lines, NaID absorption lines and $\text{H}\beta$ absorption lines, and two continuum fluxes (at 4861\AA and 6563\AA) are listed in Table 4. The typical uncertainty in the measured $\text{H}\alpha$ fluxes was 15%, as the $\text{H}\alpha$ lines often had to be deblended from an overlapping $[\text{NII}]$ emission line.

Finally, we compare our measured redshifts with those of corresponding sources in the 2Jy redshift sample. The distribution of redshift differences is plotted in Fig.8. The mean redshift difference is 0.000054 and scatter is 0.00038.

This means that our measurements agree well with these of the 2Jy catalogue.

7. DSS images

In order to be able to study the relationship between nuclear activity and degree of interaction of VLIRG in a future paper in this series, we extracted the optical images for all our objects from the CD-ROM version of Digital Sky Survey³. The contour maps using IRAF tasks, we presented in Fig.9.

8. Summary

We have presented the observation data of optical nuclear spectra and DSS images of a sample of very luminous IRAS galaxies from 2Jy catalog. In the following paper (Wu et al., 1997, Paper II), we will give the results of spectral analysis and environmental study, in the same time, address the possible model and evolutionary sequence of very luminous IRAS galaxies.

Acknowledgements. The authors would like to thank Prof. J.Y. Hu and Dr. J.Y. Wei. Their active cooperation enabled all of the observations to go through smoothly. We also thank Mr. H.J. Yan for kindly providing the extinction data for Xinglong and Prof. J.S. Chen and the rest of his group for help with the data reduction. We are also grateful to Gerard Kriss kindly providing for his procedure SPECFIT. Special Thanks to Dr. C. Young for his hard work of English revision of this paper. Finally, we are most grateful to Dr. Michael Strauss for his valuable advice. This work was partially supported by the Chinese National Science Foundation.

References

- Clements D.L. et al., 1996a, MNRAS, 279, 459
 Clements D.L. et al., 1996b, MNRAS, 279, 477
 Dennefeld M. et al., 1986, in Star Forming Dwarf Galaxies and Related Objects, eds Kunth D. et al., Edition Frontiers, p.351
 Horne K., 1986, PASP, 100, 1032, 1989
 IRAS Point Source Catalog, Version 2, 1988, Joint IRAS Science Working Group (Washington, DC: US Government Printing Office)
 Kim D.C. et al., 1995, ApJS, 98, 129
 Leech K.J. et al., 1994, MNRAS, 267, 253
 Melnick J. and Mirabel I.F., 1990, A&A, 231, L19
 Sanders D.B. et al., 1988, ApJ, 325, 74
 Soifer B.T. et al., 1986, ApJ, 303, L41
 Strauss M.A. et al., 1990, ApJ, 361, 49
 Strauss M.A. et al., 1992, ApJS, 83, 29
 Tully R.B. 1988, Nearby Galaxies Catalog, Cambridge University Press.
 Wu et al., 1997, In preparation
 Yan H.J., 1995, private communication
 Zou Z.L. et al., 1991, MNRAS, 252, 593

³ DSS CD-ROM is provided by 2.16m Telescope, Xinglong Station, Beijing Astronomical Observatory

- Zou Z.L., Xia X.Y. and Deng Z.G., 1993, Publ. Beijing Astronomical Observatory, No.23, 103
 Zwicky, F., et al. 1961-1968, Catalog of Galaxies and Clusters of Galaxies, (Pasadena:California Inst. Technology)

Table 1 VLIRGs from IRAS 2Jy Catalog

IRAS ^a	Log(L _{IR} /L _⊙)	mag	z	IRAS	Log(L _{IR} /L _⊙)	mag	z
(1)	(2)	(3)	(4)	(1)	(2)	(3)	(4)
00189+3748	11.572	15.30	0.0364	13136+6223*	11.937	15.10	0.0311
00267+3016	11.966	14.80	0.0504	13183+3423*	11.863	14.80	0.0230
00509+1225	11.772	14.00	0.0604	13299+1121	11.516	14.50	0.0317
01173+1405*	11.868	14.90	0.0312	13362+4831*	11.706	14.10	0.0275
01324+2138	11.629	15.30	0.0472	13373+0105*	11.701	13.80	0.0225
01484+2220*	11.851	13.70	0.0324	13428+5608*	12.392	15.00	0.0373
01572+0009	12.665	15.20	0.1630	13458+1540	11.821	15.00	0.0570
02071+3857	11.546	13.00	0.0179	13496+0221	11.752	15.00	0.0328
02203+3158	11.837	14.90	0.0338	13536+1836	11.611	14.80	0.0497
02222+2159	11.652	14.90	0.0338	14151+2705	11.565	15.10	0.0365
02248+2621	11.519	14.60	0.0327	14178+4927*	11.541	15.40	0.0256
02435+1253*	11.501	15.20	0.0216	14547+2448*	11.897	14.60	0.0339
02512+1446*	11.780	14.60	0.0312	14568+4504	11.501	14.60	0.0357
03117+4151	11.562	14.00	0.0235	15107+0724*	11.525	15.50	0.0131
(05084+7936)	12.170	15.80	0.0543	15163+4255*	12.072	14.90	0.0402
(05414+5840)	11.505	–	0.0148	15327+2340*	12.464	14.40	0.0182
(06538+4628)	11.490	13.70	0.0214	15425+4114	11.515	14.20	0.0317
(07062+2041)	11.559	–	0.0174	15426+4116	11.546	13.90	0.0319
07063+2043	11.570	12.60	0.0173	16104+5235*	11.687	14.50	0.0294
(07256+3355*)	11.467	14.70	0.0135	16180+3753	11.592	14.30	0.0307
08354+2555*	11.781	14.40	0.0184	16284+0411*	11.582	14.90	0.0246
08507+3520	11.811	15.00	0.0559	16504+0228*	12.028	14.70	0.0243
(09047+1838)	11.490	14.80	0.0291	16577+5900*	11.582	14.20	0.0187
09126+4432*	11.913	14.90	0.0393	16589+0521	11.637	15.50	0.0502
09168+3308	11.725	15.30	0.0499	17366+8646	11.544	14.60	0.0264
09320+6134*	12.220	15.50	0.0392	17392+3845	11.554	15.00	0.0410
09333+4841*	11.523	15.00	0.0259	17501+6825	11.829	15.20	0.0512
(09517+6954)	10.833	9.57	0.0009	18525+5518	11.683	15.50	0.0484
10203+5235	11.620	15.00	0.0322	18595+5048	11.501	15.10	0.0271
(10311+3507)	12.096	–	0.0710	19120+7320	11.624	15.10	0.0250
(10565+2448*)	12.245	16.00	0.0431	20550+1656*	12.074	15.20	0.0364
11231+1456*	11.809	15.40	0.0341	22388+3359*	11.531	15.00	0.0214
11254+1126	11.800	14.80	0.0410	22501+2427	11.723	15.30	0.0421
11257+5850	12.040	11.80	0.0104	23007+0836*	11.734	13.06	0.0162
11543+0124	11.716	15.20	0.0397	23024+1916*	11.573	15.20	0.0248
(12112+0305)	12.531	–	0.0724	23135+2516*	11.730	15.00	0.0273
12120+6838	12.029	15.40	0.0608	23254+0830*	11.568	13.60	0.0290
12251+4026	11.660	15.00	0.0371	23488+1949*	11.528	13.39	0.0142
12265+0219	12.663	13.07	0.1583	23488+2018*	11.609	14.90	0.0179
12323+1549	11.766	15.20	0.0461	23532+2513	11.795	15.00	0.0571
12540+5708*	12.636	14.10	0.0418	23594+3622	11.586	15.40	0.0321
12592+0436	11.787	15.50	0.0371				

^a The sources marked * in column (1) were also observed by Kim et al.(1995)